Diffuse interface model of the freeze-drying process of individually frozen products

Drying Technology [ISSN: 0737-3937], 38 (5-6), 758-774.
DOI: 10.1080/07373937.2019.1710711

Diffuse interface model of the freeze-drying process of individually frozen products

*Serena Bobba, Maitê Harguindeguy, Domenico Colucci, Davide Fissore**

Dipartimento di Scienza Applicata e Tecnologia, Politecnico di Torino,

Corso Duca degli Abruzzi 24, 10129 Torino, Italy.

* Corresponding author:
tel: +39-011-0904693
fax: +39-011-0904699
email: davide.fissore@polito.it

Abstract

Vacuum freeze-drying (VFD) is a dehydration method based on the sublimation of the liquid phase contained in a certain product, previously frozen, at low pressure and temperature. Since it is a time and energy consuming process, it is crucial to select the best processing conditions to minimize drying duration, thus reducing the energy requirement. Additionally, product temperature must be monitored since it plays an important role in preserving product quality. The aim of this study was to develop a Diffuse Interface Model (DIM) for *in-silico* simulation of the freeze-drying process of individually frozen products. Due to the geometrical features of the samples, and to the role of radiation in the heat transfer to the product, the usual one-dimensional approach is inappropriate. Using a DIM, each cell of the computational domain can be described as a porous solid matrix filled by ice and vapor with a time-varying composition, thus allowing the use of a fixed computational grid and making the computation effort less demanding in comparison to moving interface-based models. Drying of eggplant cubic samples was considered as case study: model parameters were estimated by fitting the experimentally measured product temperature and drying time to the calculated ones. The model was proven to be reliable in providing an accurate estimate of both the drying time and the product temperature. Therefore, it can be used for off-line process design and optimization, minimizing the experimental effort required to design and optimize the process.

Keywords

Modeling, vacuum freeze-drying, diffuse interface model, eggplant.

1. Introduction

Vacuum freeze-drying (VFD) is a low pressure and low temperature drying process based on sublimation as water removal mechanism. This requires that at the interface of sublimation, i.e. the surface where the ice turns out into the vapour phase, the temperature and pressure are below those of the triple point of the water state diagram, and that the vapour pressure of the ice is higher than the water partial pressure in the chamber as this difference acts as driving force for the vapour flux[1]-[3]. Since a high-water content may favor several degradation reactions and microbial growth, dehydration can be used as a preservation method since the reduction of the water content slows down these processes. In comparison to other drying processes, VFD is less damaging in terms of aesthetic and nutritional product qualities and, for this reason, it was used for several fruits and vegetables such as apples, bananas and carrots[4], peas, beans and spinaches[5] as well as for other products, such as fruit juices, coffee[6] and eggs[7]. Results obtained when using VFD as drying treatment are due to the low temperature along the whole process and the low oxygen partial pressure atmosphere in the drying chamber[3],[8]. Unfortunately, the process is time and energy consuming and attention should be paid in the selection of process variables, i.e. the temperature of the heating shelves and the chamber pressure, to preserve product quality and to minimize the process duration. Therefore, it is useful to perform *in silico* simulations of the sublimation process to identify off-line the temperature and pressure values that allow a complete drying of the product in a shorter time, while avoiding product overheating.

Several first-principle models were proposed in the past to describe ice sublimation, considering physical descriptions of the phenomena occurring into the system. A first group of models assumed product homogeneity and isotropy to simplify the calculations, and many times this approach appeared to be able to describe satisfactorily the process[9],[10]. However, when

the ice sublimation occurs two layers can be found in the product: an external dried layer and a frozen inner core, which gets smaller over time as the sublimation process goes on. To take into account the non-uniform composition of the product, a second group of models was developed, based on the Uniformly Retreating Ice Front (URIF) hypothesis[11]. According to the URIF approach the computational domain is divided into cells that are composed either of frozen product or of dried product. As the interface of sublimation moves over time, this implies a modification of the computational grid at each time step. This makes the model suitable for one-dimensional systems (e.g. liquid products in vials, in the pharmaceutical field, or in trays, as for freeze-drying of fruit juices), since in these cases the sublimation interface moves along just one direction, and the solution of the URIF equations is quite straightforward.

A particularly challenging case study is represented by the individually frozen products, i.e. food products cut into small pieces, and placed over the shelves of the drying chamber. In this case, the temperature and composition gradients created during the drying process do not occur in just one direction. This happens in particular when the product is heated also by radiation from chamber walls and not only from the shelf on which it lies, and a three-dimensional (3D) approach is therefore required. However, according to the URIF approach, the deformation over time of the sublimation interface requires a computational grid rearrangement to fit the shape of the sublimation front. This grid rearrangement is computationally critical in case the sublimation interface must be reshaped over three directions, thus making the URIF approach not convenient for a 3D system.

In this framework it has to be pointed out that moving boundary tracking methods on a fixed grid exist, both in 1D and in 3D, thus making the update of the computational grid not necessary to handle a moving interface. Besides, broadening of the phase change interface may be beneficial to process modeling. This is due to two main reasons:

(i) numerical handling of a sharp interface may be difficult as it induces numerical instabilities

due to material properties stiff variation over the interface;

(ii) it may account for non-smooth interfaces.

In the Literature, the concept of a multi-phase change at the interfacial zone was investigated. The mushy layer approach, for example, was introduced for describing crystallization phenomena, considering a melt phase and a crystal solid phase separated by the moving phase of transition, i.e. the solidification front, though restrictions were found in managing the kinetics of crystallization[12]. This approach also deals with convective phenomena occurring during the solidification of metal alloys or ice melting, hence the liquid-solid phase change was analyzed.[13] Nevertheless, since the sublimation involves a solid-vapor phase change, the mushy layer seems to be an unsuitable approach for describing the physics of the system considered in this study. In fact, the latter is characterized by diffusion through a porous matrix as mass transfer mechanism, instead of convection, and crystals formation is not a concern.

Warning et al.[14] applied a porous media approach to the modeling of a VFD process. The main feature of this approach is that the interface is not assumed to be "perfectly uniform", but it can also be "diffuse" in space, hence the name of Diffuse Interface Model (DIM), while the computational grid can be kept constant during the simulation of the process throughout the ice sublimation step. The main idea of this approach is that, independently of the degree of heterogeneity of the system, at a microscopic level it can be described by some effective properties, i.e. a weighted contribution of the properties of all the single phases and, thus, the usual transport equations can be solved. In a VFD system each cell of the grid is composed by a constant solid fraction, the solid matrix, plus a certain amount of water, which occupies the volume not filled by the solid matter, i.e. the porosity inside the solid matrix. The water contained in the pores can be either ice or vapor, according to the process evolution. Consequently, the composition inside the pores is time-varying, made of the sum of the ice fraction (S_i) and the vapor fraction (S_g).

The difference between the results achieved by the two approaches, URIF and DIM, is showed schematically in Figure 1. On one hand, the sublimation interface of URIF models is defined by the boundary between frozen and dried cells, thus describing a sharp moving interface (Figure 1A). On the other hand, the sublimation interface of a DIM is implicitly described by the position of cells whose ice fraction is not equal to 1 and, thus, the retreating interface is smoother (Figure 1B). In the first case, sublimation is occurring only at the sharp boundary, while, in the second approach, sublimation may occur in the whole domain, and its driving mechanism is the pressure difference between the ice vapor pressure and the water vapor pressure inside the pores.

Another approach, the phase field method, may seem powerful for describing the development of a microstructure where phase-change phenomena occur at the interface, including diffusion. However, it appears computationally challenging and some parameters, like the interface thickness, are adjustable parameters, that may be set equal to unrealistic values, and some assumption may be inconsistent with practical experience[15]. Besides, although some issues with the interface kinetics have been addressed[16], the implementation of a phase field model requires the knowledge of several coefficients, making this approach more complex method than the DIM presented in this work.

The goal of this study was to develop a mathematical model, applying the DIM approach, to describe the evolution of the temperature and of the residual amount of ice during the primary drying step of a vacuum freeze-drying process of individually frozen products, focusing on the case when radiation plays a great role in product heating. Although the word "diffusion" in the label of the model may evoke the transfer mechanism of diffusion, we kept in this manuscript the definition "diffuse interface model" as it is well established in the Literature about phase change with moving interface. The case study considered is the freeze-drying of eggplant samples, *Solanum melongena* variety, due to their high-water content and

soft texture of the solid matrix[17]. In this case, as the product investigated is heated both from the bottom by the shelf and from the chamber walls because of the radiative effects, a 3D model is proposed. Since radiation fluxes to the product may be different depending on the temperature (and features) of the emitting surfaces, for this peculiar product and arrangement 3D temperature gradients are induced in the samples, and a 2D approach, assuming axisymmetry, is not adequate. In fact, if the product is heated solely from the bottom, it would have a perfectly flat and mostly bidimensional sublimation front. This result has been proved in several studies about the freeze-drying of pharmaceutical formulations in single doses containers[18]. In this case study the radiative heat supplied to the product by the chamber walls cannot be neglected and its correct description is highly important. An URIF approach, with a sharp interface, can be numerically difficult to handle, as previously discussed and, thus, a DIM was used to describe the system. The model presented by Warning et al.[14] was thus adapted to a 3D geometry with an accurate description of the radiative fluxes. In fact, in their work a 1D model was considered, with a single radiative source and microwave heating, beside neglecting the heat supplied from the shelf. Consequently, great attention will be paid to model the radiative heat flux occurring both in a small-scale unit, used for process investigation (e.g. to determine heat and mass transfer parameters), and in an industrial-scale unit, where production may occur. The Materials and Methods section provides details about the model and the case study, pointing out the parameters of the model and providing the methodology for their estimation. In the Results section, the adequacy of the model, as well as the accuracy of the estimates of the parameters, are discussed, pointing out the necessity of a 3D approach for the selected case study.

2. Materials and Methods

2.1 Mathematical model

In the Literature, detailed models can be found and adapted to a three-dimensional domain, like the one proposed by Velardi and Barresi[18]. However, it assumes the sublimation at the interface to occur at the equilibrium, similarly to the URIF approach. Besides, the detailed model requires many parameters, while the simplified one does not consider the effect of radiation that, instead, is the main phenomenon considered in this work. This makes it not suitable for reproducing the third dimensionality of the interface evolution, which is one of the purposes of the present work. Similarly, the very comprehensive model of Liapis and Bruttini[19] could be used for the case study under investigation. Unfortunately, it involves the use of the dusty gas model to describe the vapour flux in the dried product, that requires to know the values of several parameters that may be hardly known a priori, thus requiring an extensive investigation to get their values, and the accuracy of the values that can be estimated is a serious concern.

In this work, a 3D model was used to describe the system under investigation, i.e. the cubic eggplant pieces. The mathematical model here presented consists of a differential equations system, developed from the DIM presented by Warning et al.[14], but accounting for a 3D geometry. The model was then solved through a Finite Volume Method.

Some assumptions were necessary to develop the model. First, the presence of liquid water at the end of the freezing step was neglected as well as any shrinkage phenomenon of the solid structure, as no significant evidences of it were reported experimentally. Therefore, in this study, the modelled geometric shape was considered cubic and constant over time. This approach required a description of the analytical domain, i.e. the product with a cubic three-dimensional grid, according to the reference system presented in Figure 2.

The ice sublimation flux ($\dot{I}$) was described by a non-equilibrium formula. This means that the phase change of ice into vapor takes place rapidly, but not instantaneously[20].

Consequently, there is no water thermal equilibrium between the ice-phase and the gas-phase, as Fang and Ward[21] proved experimentally. An equation found in the literature to describe the ice sublimation flux ($\dot{I}$)[14],[20] is reported in Eq. (1), where ϕ is the porosity and M_w is the molecular weight of water:

$$\dot{I} = K\left(P_{v,i} - P_v\right)\frac{M_w \phi S_v}{RT} \tag{1}$$

This equation points out that the sublimation can occur if the ice vapor pressure ($P_{v,i}$) is higher than the pressure (P_v) in each single cell of the computational domain and the gas fraction (S_v) is not zero. The non-equilibrium constant (K) is representative of the sublimation rate and it depends on the material and process conditions[22]. The phase change takes place in a much smaller time scale than the vapor diffusion phenomena through the porous matrix, which is expected to be the actual process rate controlling phenomena[20],[22]. Consequently, K is expected to be a large enough value, meaning that the resistance to the vapor diffusion at the sublimation interface is small, but not negligible. Warning et al.[14] assumed values of K in the range 10^4 - 10^6 s^{-1}, and in this study the same is considered, and K was set to 10^4 s^{-1}.

The mass balance of water vapor in the dried product of each cell of the computational domain, neglecting the convection term, is expressed by the following equation:

$$\frac{\partial c_v}{\partial t} = \frac{\partial \phi S_v \rho_v}{\partial t} = D_{eff}\nabla^2 \rho_v + \dot{I} \tag{2}$$

The description of the vapor flux in the dried product is complex as both permeation and diffusion are possible: this would require the fitting of many parameters, including those describing the Stefan-Boltzman effect of diffusion. As an example, the dusty gas model frequently used to model the vacuum freeze-drying of pharmaceutical formulations has 4 parameters. Unfortunately, it is almost impossible to know a priori the values of these parameters and, thus, in this work the mass transfer inside the porous matrix was modelled as an effective mechanism in the form of a diffusion term. It could be described as an effective

convective term provided that the equations required to model both permeability and the viscosity of the gas flow are available. In fact, if, as in this case, the partial pressure gradient can be confounded with the total pressure gradients, the two descriptions could be considered equivalent. The reliability of the equations available in Literature for the description of these terms in a transition regime is questionable and at the end one or more parameters would have had to be adjusted in all cases.

Expanding the derivative on the left side of equation (2) leads to:

$$\frac{\partial \phi S_v \rho_v}{\partial t} = \phi S_v \frac{\partial \rho_v}{\partial t} + \phi \rho_v \frac{\partial S_v}{\partial t} = \phi \left(1 - S_i\right) \frac{\partial \rho_v}{\partial t} - \phi \rho_g \frac{\partial S_i}{\partial t} \tag{3}$$

By its own definition:

$$\dot{I} = -\frac{\partial c_i}{\partial t} = -\phi \rho_i \frac{\partial S_i}{\partial t} \tag{4}$$

where c_i is the ice concentration in the cell, while the ice density is considered constant. The derivative of the ice volume fraction can thus be written as:

$$\frac{\partial S_i}{\partial t} = -\frac{\dot{I}}{\phi \rho_i} \tag{5}$$

Considering equations (3) and (5), equation (2) may be written as:

$$\frac{\partial \rho_v}{\partial t} = \frac{1}{\phi \left(1 - S_i\right)} \left(-\frac{\rho_v}{\rho_i} \dot{I} + D_{eff} \nabla^2 \rho_v + \dot{I} \right) \tag{6}$$

This equation considers the accumulation of water vapor, its generation at the interface of sublimation, and its diffusion in the dried matrix according to the composition gradient.

The vapor flow regime in the porous media can be affected by some deviation from the continuum assumption, according to the freeze-drying conditions[23]. In fact, in case the Knudsen number (*Kn*), used to establish in which regime the flow takes place, is higher than 1, Knudsen diffusivity should be considered. For the case study under investigation, *Kn* is surely larger than 1, as the values of pore diameter of eggplant samples that can be found in the

Literature range from 20 to 55 μm[24], thus resulting in *Kn* ranging (roughly) from 1 to 10. The Knudsen diffusivity that has to be considered is related to the effective diffusivity by the void fraction and the tortuosity of the porous matrix[25]. Because of the uncertainty on these parameters, D_{eff} was estimated by looking for the best fit between experimental data and those obtained from simulations, as it will be discussed ahead.

Assuming that the relationship between partial pressure and vapor density obeys to the perfect gas equation, equation (1) can be rewritten as equation (7)[26]:

$$\dot{I} = K\left(\rho_{v,i} - \rho_v\right) \tag{7}$$

It appears that the sublimation flux is proportional to the difference between the vapor density at the interface of sublimation ($\rho_{g,i}$) and in the gas phase (ρ_v). For computing $\rho_{v,i}$ through the ideal gas law, the ice partial pressure ($P_{v,i}$) is required. Equation (8) shows a simplified equation given by Fissore et al.[27] that was used in this study:

$$P_{v,i} = e^{-\frac{6140.4}{T}+28.916} \tag{8}$$

The heat balance of each cell of the computational domain used in the model is given by equation. (9):

$$\frac{\partial T}{\partial t} = \frac{1}{\rho_{eff} c_{p,eff}}\left(k_{eff}\nabla^2 T - \lambda \dot{I}\right) \tag{9}$$

The same set of equations presented above can be applied to all the domain cells, as long as the effective proprieties are used:

$$\rho_{eff} = \rho_s\left(1-\phi\right) + \rho_i S_i \phi + \rho_v\left(1-S_i\right)\phi \tag{10}$$

$$c_{p,eff} = \frac{\rho_s\left(1-\phi\right)c_{p,\mathrm{s}} + \rho_i \phi S_i c_{p,\mathrm{i}} + \phi\left(1-S_i\right)\rho_v c_{p,v}}{\rho_{eff}} \tag{11}$$

$$k_{eff} = \left(1-\phi\right)k_s + k_i \phi S_i \tag{12}$$

The ice properties, i.e. thermal conductivity, density and specific heat, were calculated as a

function of temperature by using the equations proposed by Fukusako[28]:

$$k_i = 1.6\left(1.91 - 8.66\cdot10^{-3}\left(T - 273.15\right) + 2.97\cdot10^{-5}\left(T - 273.15\right)^2\right) \quad (13)$$

$$c_{p,i} = 185 + 6.89T \quad (14)$$

$$\rho_i = 917\left(1 - 1.17\cdot10^{-4}\left(T - 273.15\right)\right) \quad (15)$$

The porosity was calculated weighting the samples before and after the drying process, applying the same procedure adopted by Sereno et al.[29].

According to Warning et al.[14], the vapor specific heat capacity was assumed constant, while the specific heat capacity of the solid product and its thermal conductivity were estimated to obtain a good fit of the product temperature profiles. Indeed, any relations found in the Literature to describe them would not give reliable results, due to the non-compact eggplant structure and the presence of seeds[30] which makes the product extremely heterogeneous.

2.2 Boundary and initial conditions

In order to solve the model composed by equations (1)-(9), adequate boundary and initial conditions are required. The initial sample temperature (T_0) was set equal to the freezing temperature. The initial gas density ($\rho_{v,0}$) was calculated assuming an ideal gas behavior, thanks to the low-pressure condition[31] and considering water vapor to be the only chemical species in the chamber. To avoid numerical instability in equation (6), the ice fraction at time zero ($S_{i,0}$) has to be smaller than one. Indeed, Warning et al.[14] recommend a value in the 0.25-0.99 range and in the present study a value equal to 0.8 was estimated, according to Tchigeov empirical relation[32], using the physical properties of eggplants reported in the USDA database[33].

The boundary conditions regarding product temperature were developed considering that the product is heated both from the shelf and from the chamber walls, which are at higher temperature. Heat exchange occurs from the shelf to the bottom face of the cube through several

heat transfer mechanisms, e.g. conduction in the contact points between shelf and the eggplant sample, and the conductive-radiative phenomena occurring in the space between the eggplant sample and the shelf. Therefore, the sample is considered to be heated by the shelf through the bottom face by a heating flux proportional to the difference between the shelf temperature and the product temperature, multiplied by the heat transfer coefficient K_v. This coefficient is an overall coefficient considering the heating mechanisms presented above and, as such, it was estimated looking for the best fit between calculated and experimentally measured data.

The other five faces of the sample are heated by radiation from the walls of the chamber. It must be pointed out that the radiative heat transfer can play a relevant role in the heat transfer to the product and might be responsible of a surface temperature higher than that of the heating shelf. This issue has to be carefully considered, due to the role of product temperature in the preservation of nutritional features of the food processed.

In order to compute the radiative heat flux, it is required to know first the view factors values and the effective emissivity (ε) of the surfaces involved. The latter depends on the specific materials of the surfaces, that is of both the emissivity of the product and of the stainless steel of the shelves[34]. Furthermore, the emissivity has an intrinsic dependence from the temperature, that is from the operating conditions. Given all the uncertainties in the measurement of the effective value, an approximate mean value of 0.9 was obtained for ε and assumed to remain constant across the whole set of experimental conditions tested.

Regarding the view factors, several hypotheses are needed to estimate them, as an exact evaluation would be computationally too demanding. To calculate the view factors, only the most significant contributions given by some areas of the chamber walls were considered. The upper face of the sample was considered to be irradiated by the upper shelf surface and by the four vertical chamber walls surrounding the batch, while each side of the cube was considered to be irradiated by an area of the shelf as large as the cube side itself (Figure 3). This last

approximation comes from the layout adopted in the experimental campaign for placing the samples on the shelf, as the distances between samples were comparable to their own side length.

The view factors were calculated considering three geometrical configurations, according to the radiative heat contributions previously listed. The nomenclature used in the following equations (16) - (30) refers to geometrical parameters illustrated in Figure 4.

In order to calculate the view factor regarding the heat flux from the upper shelf to the product top face ($F_{T,T}$), the geometrical configuration illustrated in Figure 4A is considered, and the view factor for parallel square planes (equations (16)-(21))[35] is used:

$$q_1 = \frac{L_1}{D}\left(1+\frac{L_1}{L_2}\right) \tag{16}$$

$$q_2 = \frac{L_1}{D}\left(1-\frac{L_2}{L_1}\right) \tag{17}$$

$$\alpha = \ln \frac{\left[\left(\frac{L_1}{D}\right)^2\left(1+\left(\frac{L_2}{L_1}\right)^2\right)+2\right]^2}{\left(q_2{}^2+2\right)\left(q_1{}^2+2\right)} \tag{18}$$

$$\beta = \sqrt{q_2{}^2+4}\left[q_2 \tan^{-1}\frac{q_2}{\sqrt{q_2{}^2+4}} - q_1 \tan^{-1}\frac{q_1}{\sqrt{q_2{}^2+4}}\right] \tag{19}$$

$$\gamma = \sqrt{q_1{}^2+4}\left[q_1 \tan^{-1}\frac{q_1}{\sqrt{q_1+4}} - q_2 \tan^{-1}\frac{q_2}{\sqrt{q_1{}^2+4}}\right] \tag{20}$$

$$F_{A_1,A_2} = \frac{1}{\pi\left(\frac{L_1}{D}\right)}\left(\alpha+\beta+\gamma\right) \tag{21}$$

Therefore, in the model $F_{T,T} = F_{A_1,A_2}$.

As far as the view factors related to the radiation between each chamber vertical wall and the product top face ($F_{L,T}$, $F_{R,T}$, $F_{F,T}$, $F_{B,T}$) have to be calculated, the geometrical

configuration shown in Figure 3B is considered, corresponding to perpendicular planes without any common sides (equations (22)-(24))[36]. In this case:

$$X = \frac{a}{b} \tag{22}$$

$$Y = \frac{c}{b} \tag{23}$$

$$F_{A_1,A_3} = \frac{1}{2\pi}\left(\tan^{-1}\frac{1}{Y} - \frac{Y}{\sqrt{X^2+Y^2}} \tan^{-1}\frac{1}{\sqrt{X^2+Y^2}} \right) \tag{24}$$

According to literature, the geometrical configuration at the basis of previous equation considers half of the radiating surface, i.e. half of the radiating chamber walls (as represented in Figure 4B by the dashed line). Therefore, it has to be multiplied by 2 to consider the effect of the entire chamber walls. In the model we have that $F_{R,T} = F_{L,T} = F_{F,T} = F_{T,T} = F_{A_1,A_3}$.

In order to calculate the view factors $F_{S,L}$, $F_{S,R}$, $F_{S,F}$, $F_{S,B}$ needed to evaluate the radiating heat flux reaching the side faces from the shelf (Figure 3C), the perpendicular rectangular planes with a common side were considered (equations (25) - (30))[37]. In this case:

$$W = \frac{f}{e} \tag{25}$$

$$h = \frac{g}{e} \tag{26}$$

$$p_1 = \frac{\left(1+W^2\right)\left(1+h^2\right)}{1+W^2+h^2} \tag{27}$$

$$p_2 = \frac{W^2\left(1+W^2+h^2\right)}{\left(1+W^2\right)\left(W^2+h^2\right)} \tag{28}$$

$$p_3 = \frac{h^2\left(1+W^2+h^2\right)}{\left(1+h^2\right)\left(W^2+h^2\right)} \tag{29}$$

$$F_{A_4,A_5} = \frac{A_4}{\pi W A_5}\left(W\tan^{-1}\frac{1}{W} + h\tan^{-1}\frac{1}{h} - \left(h^2+W^2\right)^{0.5}\tan^{-1}\frac{1}{\left(h^2+W^2\right)^{0.5}} + 0.25\ln\left(p_1 {p_2}^{W^2} {p_3}^{H^2} \right) \right)$$

(30)

Once the view factors were calculated, the radiative heat flux reaching each face of the sample was calculated by using the following equations:

$$\dot{Q}_L = \sigma\varepsilon F_{S,L} A_S \left(T_S^4 - T^4\right) \tag{31}$$

$$\dot{Q}_R = \sigma\varepsilon F_{S,R} A_S \left(T_S^4 - T^4\right) \tag{32}$$

$$\dot{Q}_F = \sigma\varepsilon F_{S,F} A_S \left(T_S^4 - T^4\right) \tag{33}$$

$$\dot{Q}_B = \sigma\varepsilon F_{S,B} A_S \left(T_S^4 - T^4\right) \tag{34}$$

$$\begin{aligned}\dot{Q}_T = {} & \sigma\varepsilon F_{L,T} A_L \left(T_L^4 - T^4\right) + \sigma\varepsilon F_{R,T} A_R \left(T_R^4 - T^4\right) + \sigma\varepsilon F_{F,T} A_F \left(T_F^4 - T^4\right) + \\ & + \sigma\varepsilon F_{B,T} A_B \left(T_B^4 - T^4\right) + \sigma\varepsilon F_{T,T} A_T \left(T_T^4 - T^4\right)\end{aligned} \tag{35}$$

It is therefore necessary to know the values of the chamber wall temperatures (T_L, T_R, T_F, T_B), besides the temperature of the lower surface of the upper shelf.

The boundary condition regarding the gas density considers the vapor flux from the product surface to the chamber. The vapor propagates through the porous matrix to the surface, and then through the vacuum chamber. The vapor propagation in different materials is characterized by different diffusivities. Moreover, in the physical system under investigation, the vapor flux faces additional resistances while moving from the chamber to the condenser. However, their contribution is minimal, and the estimation of an additional parameter, i.e. the vapor diffusivity in the vacuum atmosphere, would increase the number of unknown parameters to be estimated. In this work, an approach based on the use of the "ghost cells" [38], a shell of cells around the product that can be characterized with specific properties values, was preferred. In this study, the ghost cells were modelled as a layer around the product where the vapor diffusivity is the same as inside the porous matrix. Hence, the diffusivity here considered is an effective one, considering the contribution of the several transport phenomena that describe the vapor flux from the sublimation interface to the drying chamber. The mass transfer resistance

due to the flow from the chamber to the condenser was neglected. The vapor flux boundary condition from the surface to the chamber is thus given by the following equation:

$$J_D = -\frac{D_{eff}}{A}\left(\rho_{ext} - \rho_v\right) \tag{36}$$

Since the contact with the shelf might prevent diffusive phenomena, the face laying on the shelf was assumed impermeable to the vapor flux and, thus, A is given by the total area of the 5 faces exposed to the chamber. The density of the atmosphere (ρ_{ext}) in the camber was calculated from ideal gas law at chamber pressure, assuming that it is composed only by water vapor.

Table 1 summarizes the values of physical properties used in the model equations.

2.3 Experimental investigation

Data collected during the freeze-drying of eggplant samples were used to estimate model parameters (K_v and D_{eff}) and to validate the previously presented model.

Fresh eggplants were bought in a local market in Turin (Italy9 and processed daily. It is worth noting that this product is highly heterogeneous, due to the high seasonal variability and differences between each cultivar. Furthermore, the eggplant samples composition is not homogeneous due to the presence of seeds in the vegetable flesh, affecting the data collected and natural variability of the product[39].

Eggplants were freeze-dried in a LyoBeta 25 unit by Telstar (Terrassa, Spain), which is a pilot-scale equipment with 0.2 m^3 chamber volume. The equipment has an external condenser that operates at approximately -80°C, with a maximum ice capacity of 40 kg. The shelf temperature was set at -50°C for 4 hours during the freezing step. After that, different process variables, i.e. shelf fluid temperature and chamber pressure, were tested to evaluate their influence over product temperature and. time required to completely removed the frozen water. In detail, the tests that were carried out are the followings: test #A1 and #A2 at -30°C and 30 Pa, test #B at -15°C and 20 Pa, test #C at 0°C and 30 Pa.

To monitor the product superficial temperature an infrared (IR) thermography-based sensor (FILR A35) presented by Lietta et al.[40] was employed, while the temperature inside the samples was measured by means of T-type thermocouples (Tersid, Milano, Italy). The temperatures of the chamber walls and of the shelf were measured during each freeze-drying test also by T-type thermocouples, which were stick at the chamber walls and on the shelf by means of a thermal conductive tape. One last thermocouple was left unbounded in the chamber to measure the temperature of the gas phase in the chamber.

To estimate the end point of the drying phase, pressure measurements were taken by a Pirani (P_P) gauge (PSG-101-S, Inficon, Bad Ragaz, Switzerland) and a capacitance manometer (P_B), both installed in the drying chamber. Their ratio (P_P/P_B) decrease was regarded as an evidence for end of drying[41]. The middle point of the decreasing curve trend may be considered as a representative end point, although also the onset of the decreasing part of the curve may be assumed to be representative of the ending point of the primary drying stage.

Cubic eggplant samples were processed. A cube of side length equal to 9 mm constitutes the computational domain to reproduce the actual shape of the eggplant samples being freeze dried in the experiments. The model was implemented on the numerical computing environment MATLAB R2018a, by MathWorks®. The cubic domain was divided into an 8 x 8 x 8 units grid. Larger number of cells did not result into any appreciable accuracy increment, while requiring much longer computational times.

2.4 Estimation of model parameters and model validation

For estimating the mass and heat transfer coefficient values, the surface temperature profiles in five samples were selected from each run. The temperature on the product surface was recorded throughout the whole primary drying stage by the infrared camera. Five samples were selected randomly in each batch, in the central position, and the temperature in the center of a lateral

face, the one standing in front of the camera, was recorded. Then, the values of K_v and D_{eff} were estimated looking for the best fit between calculated and measured values of product temperature. A MATLAB R2018a script was used to this purpose.

Model validation was carried out in three different ways:

i. by calculating the evolution of product temperature in a different run, where the operating conditions were not varied (e.g. in run #A2 with respect to run #A1), or in a run where one of the parameters was expected to remain the same (e.g. in run #C the value of K_v is expected to remain the same of run #A, being the pressure the same), and comparing the calculated trends with the measured ones;

ii. by comparing the measured and the calculated values of product temperature in a different point, e.g. at the bottom of the sample where a thermocouples was placed to catch this value (in this case, care must be paid when evaluating the results as the uncertainty in thermocouple position may be relevant);

iii. by comparing the drying time calculated through mathematical modeling with the curve of the ratio between the Pirani and the capacitance manometers: although there is a certain uncertainty when using this curve to infer the ending point of the sublimation stage, it is required that the calculated ending point of the primary drying falls in the range identified by the onset and the offset of the curve[41].

3. Results and discussion

This section is organized as follows: at first, the proposed model is validated, and its main parameters are estimated from experimental tests. Then, the role of radiation on the heat transfer to the product is discussed.

3.1 Model validation and parameters estimation

Using the method described in the Materials and Methods section, model parameters K_v and D_{eff} were estimated using data obtained in run #A1 (-30°C and 30 Pa). Five temperature profiles, each referring to a different sample, were randomly selected among those obtained with the IR camera. Values of K_v and D_{eff}, calculated to obtain the best fit between experimentally measured and calculated values of the temperature at the center of the lateral surface of each cube, are shown in Table 2, where the mean value and the standard deviation of both parameters are also shown. It is worthwhile noticing that the order of magnitude of K_v and D_{eff} are similar to those reported in the Literature for other vacuum freeze-drying processes.[42],[43]

Figure 5 shows a comparison between the calculated values of product temperature at the top surface of the product (in central position), using the mean values of model parameters, and the experimentally measured values from a second run (#A2), carried out with the same operating conditions used to determine the model parameters (run #A1). Results evidenced the good agreement between the calculated and the measured temperature on the surface of the product (Figure 5, graph A). It has to be remarked that the temperature on the surface of each sample can be the highest of the sample itself due to radiation effects, and this has to be carefully calculated, in the stage of process design, to avoid product overheating. Figure 5, graph B, shows also the comparison between the calculated temperature at the bottom of the sample, in central position, and the value measured through the thermocouples placed in the sample. Considering all the uncertainties related to the measurement of the temperature at the bottom of a small cube using a thermocouple, the agreement looks rather good. In fact, the exact positioning of the tip is a major source of uncertainty, and in some case the cable might slightly lift the cube from the perfect contact with the shelf that is implicitly assumed by the model. Considering the intrinsic variability in the sample, i.e. different stiffness, ripeness, number of

seeds (that is the heterogeneity of the sample) and, indeed, mild differences in the preparation of the samples, the fact that two measurements obtained in different runs agree, although not perfectly, is a good result.

With respect to the estimate of the ending time, it is necessary to compare the measured P_P/P_B ratio, with the calculated ratio between the residual amount of ice in the product (m_i) and the ice mass at the beginning of the drying ($m_{i,0}$). Results obtained for run #A2 are shown in Figure 6. When the ice ratio ($m_i/m_{i,0}$) becomes equal to zero, after 15 hours from the onset of the primary drying in this run, drying is obviously completed. This value is in excellent agreement with the midpoint of the P_P/P_B curve, thus providing an additional validation of model calculations.

Other tests were carried out to assess the adequacy of the proposed model to describe the evolution of the drying process. Figure 7 shows the results obtained in run #B, carried out at -15°C and 20 Pa. In this case the estimated values of model parameters are 14 W m^{-2} $°C^{-1}$ for K_v, and $2.0 \cdot 10^{-4}$ m^2 s^{-1} for D_{eff}. The agreement between the calculated and the measured values of surface product temperature is very good, as shown in Figure 7, graph A, in particular with respect to the highest temperature. Only minor discrepancies can be found in the initial part of the temperature profile. This may be due to the uncertainty of the various physical properties that are needed for process simulation, plus to the heterogeneity of the product itself, which makes the vegetable sample subjected to non-uniform behavior. Some fluctuations in the calculated temperature profile may also be due to numerical issues caused by the Finite Volume Method adopted. As far as drying time is concerned, in Figure 7, graph B, the value calculated considering $m_i/m_{i,0}$ falls in the range of time where the P_P/P_B curve is decreasing and, thus, may be considered acceptable. As expected, the calculated value of the overall heat transfer coefficient K_v is lower with respect to that obtained in run #A1 due to the lower pressure. In fact, chamber pressure affects the conduction in the gas layer between the shelf and the product

laying upon it, and the lower is the pressure, the lower is the heat conductivity of the gas, strongly decreasing the value of K_v, being the effect of the shelf temperature almost negligible[42]. The effect of the operating conditions on D_{eff} are much more difficult to be explained, due to the flow regime in the dried matrix, and to the fact that the operating conditions affect also the temperature in the channels where the vapor flows.

A further validation was carried out through run #C, carried out at 0°C and 30 Pa. In this case chamber pressure was the same of runs #A1 and #A2, while the temperature of the shelf was increased from -30°C to 0°C. Results are shown in Figure 8 where, again, the comparison between calculated and measured value of product temperature at the top surface (graph A) and the comparison between $m_i/m_{i,0}$ and P_P/P_B curves (graph B) are shown. The conclusions are the same presented for run #B. In this case we carried out two different simulations: in the first, we used the same values of model parameters that were estimated in run #A1 (see Table 2). This was due to the fact that being chamber pressure the same, then the value of the heat transfer coefficient K_v is not expected to change. Besides, as the temperature of the product is expected to show a limited change, then also D_{eff} is not expected to change. Results are shown in Figure 8 as symbols. In a second calculation, we optimized the values of D_{eff} and K_v for this test, and results are shown as dashed lines in the Figure. The optimized values of model parameters are 27 W m^{-2} $°C^{-1}$ for K_v and $2.5 \cdot 10^{-4}$ m^{-2} s^{-1} for D_{eff}. Results shown in Figure 8 evidences the satisfactory prediction capacity of the model: using in fact the values of model parameters estimated in run #A1, the initial transient evolution of the temperature and the steady-state value appear to be properly evaluated, as well as the drying time. Little improvement is obtained when model parameters are optimized for this specific case study: focusing on these optimized values, it has to be pointed out that, as expected, the value of K_v is not significantly different from that obtained in run #A1 carried out at the same pressure of run #C, considering that chamber pressure, for the selected case study, is the main parameter

affecting the value of K_v. Also, the value of D_{eff} is not significantly different. This can be explained considering that in Knudsen regime the Knudsen diffusivity is proportional to the square root of the temperature of the vapor[43]. Obviously, the temperature of the vapour changes from the value at the interface of sublimation (where it is lower), to the value at the interface with the drying chamber (where it is higher). The latter is directly measured through the IR camera, and the former can be estimated using the mathematical model. Using a simplified approach, the temperature at the interface of sublimation may be assumed to be equal to the value measured by the thermocouple at the bottom center of the sample as the temperature gradients in the frozen product are almost negligible. This way, it is possible to evaluate at each time instant the mean temperature in the dried product (corresponding to the mean temperature of the vapor flowing in the pores) in both cases. The average values over time of these temperatures are 246 K and 269 K respectively in runs #A and #C. Once elevated to the power of 0.5, their ratio was found equal to 1.04, while the ratio of the values of D_{eff} estimated for runs #A and #C was found equal to 1.08, thus motivating the observed effect of the operating conditions on this parameter.

Focusing on runs #A and #B that are different for both temperature and pressure, again the different temperature of the product is expected to have a negligible effect on the value of D_{eff}. The effect of the pressure is much more complex to be evaluated. In particular, it seems that at a lower pressure (20 Pa vs. 30 Pa) the value of D_{eff} decreases as well ($2.0 \cdot 10^{-4}$ m^2s^{-1} vs. $2.66 \cdot 10^{-4}$ m^2s^{-1}). Although in Knudsen regime no effect of pressure is expected, in this case, due to the complex porous structure of the sample processed, the flow regime may vary between the transition and the Knudsen regime. Moreover, this parameter is an effective one, which accounts for several physical parameters.

3.2 Role of radiative heat

To point out the effectiveness of using a DIM, the existence of a complex sublimation interface, thus of a 3D ice concentration gradient, is evaluated and discussed. From Figure 5, graph A, it can be easily seen that the temperature on the product surface, monitored during the run, was considerably higher than the temperature at the bottom, graph B. This is a clear evidence of the radiative heat exchange from the chamber to the samples, being responsible of the temperature increase on the product surface.

Indeed, the radiative heat plays a major role among all the heating phenomena involving the product. From simulation of run #A2, the heating flux through the samples bottom face was calculated over the drying time, equal to about 90 J. Given the latent heat of sublimation of the ice and its initial amount, the energy needed for the total sublimation was calculated approximatively equal to 1.0 kJ. Therefore, the heat received from the shelf turned out to be just a minor fraction (about 9%) of the total one. Radiation represents about 91% of the total heat transfer to the system and, thus, its specific influence on the product development could not be neglected. Analogously, the heating flux from the shelf was calculated for runs #B and #C, respectively equal to about 12% and 35% of the total heat required for ice sublimation.

It worth notice that the two side walls and the front wall of the equipment differ of a couple of degrees, i.e. from 2 to 4°C, and might be merged in a single term. The door follows a completely different trajectory. The number of radiative terms could be reduced to two, and only two temperatures, namely T_B and either T_L, T_R or T_F should be measured to obtain a simplified characterization of the chamber.

As a consequence of the significant radiative phenomena, it is reasonable that an important 3D temperature gradient is established inside the product, leading to a gradient of ice vapor pressure, thus to different sublimation driving forces along a product section. The planes monitored in order to provide an idea of the sublimation interface on a horizontal profile, were the second, the fourth and the sixth, being the second close to the lower part of the sample, and

the sixth to the upper part. As shown in Figure 9, these profiles are different from each other, evidencing that there is not a sharp interface between the frozen and the dried product, thus further motivating the need for a 3D model.

In fact, the URIF model assumes the thermal equilibrium at the sublimation front, that is no mass transfer resistance between the frozen surface and the gas phase. This is a reliable assumption when the sublimation front is perfectly flat as proved by the models of the VFD for pharmaceutical solutions based on this assumption. Yet, although minor, it cannot be neglected a priori and must be accounted to correctly describe the dimensionality of the sublimation front. The fact that K is a quite large number clearly states that this resistance is minor or, at least, lower than the resistance to mass transfer due to the flow in the porous matrix. Nevertheless, being the total sublimation rate proportional to S_g, when the ice fraction is small the whole product $S_g \cdot K$ will be small and the resistance to mass transfer at the ice-vapor interface consistent.

The 3D sublimation interface is made evident when the ice fraction on a vertical section of the cubic domain in represented, proving the effectiveness of the DIM approach. In fact, in Figure 10 the cells where the ice fraction is decreasing represent the actual sublimation interface. By representing them in the same vertical section over different times, the development of the sublimation interface can be described, moving progressively from the upper and lateral faces, to an inner core in correspondence of the bottom face. This spatial-over time evolution agrees with what expected from the radiative heat fluxes and vapor flux bottom condition implemented.

4. Conclusions

Mathematical modeling is well known to be a powerful tool for process design and optimization, provided that it effectively accounts for the heat and mass transfer phenomena occurring in the system considered. In this paper a 3D model was presented to describe the vacuum freeze-drying of cubic samples of individually frozen products. Heat transfer mainly occur by radiation from chamber walls and, thus, the usual one-dimensional model derived from URIF approach cannot be used, and a diffuse interface model appears to be the most adequate approach. Only two parameters must be estimated experimentally, namely K_v and D_{eff}, using the measured values of product temperature at the surface of the product. The well-known effect of the pressure on the K_v value was found to be correctly addressed by the model, as well as the negligible effect of the temperature on the effective water vapor diffusivity. The model is able to accurately calculate the temperature of the product throughout the primary drying stage, and in particular the surface temperature, that is usually the highest, besides providing acceptable estimates of the drying time.

Finally, the amount of heat received by the product from the shelf estimated, underlining the relevance of radiative phenomena and the retreating of the sublimation interface, was plotted as modeled to display the significance of the gradients through the sample.

The proposed model is a powerful tool for process design as it allows investigating, off-line, the effect of the temperature of the radiating surfaces on product temperature and drying duration for a given chamber pressure. Moreover, in case of model parameters having been estimated at different temperature and pressure, also the chamber pressure may be included as operating variable to be optimized.

Future development of this study might consider a deeper investigation on the influence of the operating conditions on the kinetic parameters of the product, as well as the application of this DIM to the modeling of the vacuum freeze-drying of pharmaceuticals and biopharmaceuticals in vials, as well as to the modeling of the atmospheric freeze-drying

processes.

List of Symbols

a	parameter used in Eq. (22)
A	external area of the product, m^2
A_F	chamber wall area considered for evaluating the radiative flux in front of the product, m^2
A_L	chamber wall area considered for evaluating the radiative flux on the left of the product, m^2
A_B	chamber wall area considered for evaluating the radiative flux on the back of the product, m^2
A_R	chamber wall area considered for evaluating the radiative flux on the right of the product, m^2
A_S	area of the shelf considered in the evaluation of the radiative flux, m^2
A_T	upper shelf are considered in the evaluation of the radiative flux, m^2
b	parameter used in Eq. (22)
c	parameter used in Eq. (23)
$c_{p,eff}$	effective heat capacity, J kg^{-1} K^{-1}
$c_{p,i}$	heat capacity of the ice, J kg^{-1} K^{-1}
$c_{p,s}$	heat capacity of the solid, J kg^{-1} K^{-1}
$c_{p,v}$	heat capacity of the vapour phase, J kg^{-1} K^{-1}
D	parameter used in Eq. (16)
D_{eff}	vapor effective diffusivity, m^2 s^{-1}
e	parameter used in Eq. (25)
$F_{B,T}$	view factor from back wall to top product face
$F_{F,T}$	view factor from front wall to top product face

$F_{L,T}$	view factor from left wall to top product face
$F_{R,T}$	view factor from right wall to top product face
$F_{S,B}$	view factor from shelf to back product face
$F_{S,F}$	view factor from shelf to frontal product face
$F_{S,L}$	view factor from shelf to left product face
$F_{S,R}$	view factor from shelf to right product face
$F_{T,T}$	view factor from the upper shelf to top product face
f	parameter used in Eq. (25)
g	parameter used in Eq. (26)
h	parameter calculated through Eq. (26)
$\dot{I}$	sublimation flux, kg m^{-3} s^{-1}
J_D	vapor flux from the product to the chamber, kg $s^{-1}m^{-2}$
K	non-equilibrium constant, s^{-1}
K_v	heat transfer coefficient, W m^{-2} K^{-1}
k_{eff}	effective heat conductivity, W m^{-1} K^{-1}
k_i	heat conductivity of the ice, W m^{-1} K^{-1}
k_s	heat conductivity of the solid, W m^{-1} K^{-1}
Kn	Knudsen number
L_1, L_2	parameters used in Eqs. (16) and (17)
M_w	water molecular weight, kg mol^{-1}
m_i	residual ice amount, kg
$m_{i,0}$	ice amount at the beginning of the process, kg
p_1	parameter calculated through Eq. (27)
p_2	parameter calculated through Eq. (28)
p_3	parameter calculated through Eq. (29)

P_v	pressure in the pores, Pa
$P_{v,i}$	ice vapor pressure, Pa
P_B	Pressure measured through capacitance gauge, Pa
P_P	Pressure measured through the thermal conductivity gauge, Pa
$\dot{Q}_B$	radiative heating flux reaching the product back face, W
$\dot{Q}_F$	radiative heating flux reaching the product frontal face, W
$\dot{Q}_L$	radiative heating flux reaching the product left face, W
$\dot{Q}_R$	radiative heating flux reaching the product right face, W
$\dot{Q}_S$	radiative heating flux reaching the product bottom face, W
$\dot{Q}_T$	radiative heating flux reaching the product top face, W
q_1, q_2	parameters calculated through Eqs. (16) and (17)
R	ideal gas constant, J mol^{-1} K^{-1}
S_i	ice fraction
$S_{i,0}$	initial ice fraction
S_v	vapor fraction
T	product temperature, K
T_0	initial product temperature, K
T_F	temperature of the chamber wall in front of the product, K
T_L	temperature of the chamber wall at the left of the product, K
T_B	temperature of the chamber wall on the back of the product, K
T_R	temperature of the chamber wall at the right of the product, K
T_S	temperature of the shelf, K
T_T	temperature of the upper shelf, K
t	time, s

X	parameter calculated through Eq. (22)
x	axial coordinate
Y	parameter calculated through Eq. (23)
y	axial coordinate
W	parameter calculated through Eq. (25)
z	axial coordinate

Greeks

α	parameter calculated through Eq. (18)
β	parameter calculated through Eq. (19)
γ	parameter calculated through Eq. (20)
ε	effective emissivity
λ	heat of sublimation, J kg^{-1}
ϕ	porosity
ρ_{eff}	effective density, kg m^{-3}
ρ_{ext}	vapor density in the chamber, kg m^{-3}
ρ_i	ice density, kg m^{-3}
ρ_v	water density in the vapour phase, kg m^{-3}
$\rho_{v,i}$	water vapor density at the interface of sublimation, kg m^{-3}
$\rho_{v,0}$	initial gas density, kg m^{-3}
σ	Stefan-Boltzman constant, W m^{-2} K^{-4}

References

[1] Meryman, H. T. Freeze-Drying without Vacuum. *Science.* **1959**, *130*, 628–629.

[2] Claussen, I. C.; Ustad, T. S.; Strømmen, I.; Walde, P. M. Atmospheric Freeze Drying: A Review. *Drying Technol.* **2007**, *25* (6), 947–957. DOI: 10.1080/07373930701394845.

[3] Berk, Z. Freeze Drying (Lyophilization) and Freeze Concentration. In *Food Process Engineering and Technology*; 1st ed.; Berk, Z., Ed. Elsevier: Amsterdam, **2013**; pp. 567–581.

[4] Krokida, M. K.; Karathanos, V. T.; Maroulis, Z. B. Effect of Freeze-Drying Conditions on Shrinkage and Porosity of Dehydrated Agricultural Products. *J. Food Eng.* **1998**, *35* (4), 369–380. DOI: 10.1016/s0260-8774(98)00031-4.

[5] Oetjen, G.W.; Haseley, P. *Freeze-Drying*, 2nd ed.; Wiley: Weinheim, **2004**.

[6] Ishwarya, S. P.; Anandharamakrishnan, C. Spray-Freeze-Drying Approach for Soluble Coffee Processing and its Effect on Quality Characteristics. *J. Food Eng.* **2015**, *149*, 171–180. DOI: 10.1016/j.jfoodeng.2014.10.011.

[7] Wang, Y.; Zhang, M.; Adhikari, B.; Mujumdar, A. S.; Zhou, B. The Application of Ultrasound Pretreatment and Pulse-Spouted Bed Microwave Freeze Drying to Produce Desalted Duck Egg White Powders. *Drying Technol.* **2013**, *31* (15), 1826–1836. DOI: 10.1080/07373937.2013.829851.

[8] Fissore, D.; Velardi, S. Freeze Drying: Basic Concepts and General Calculation Procedures. In *Operations in Food Refrigeration*, Mascheroni R. H., Ed. Taylor & Francis Group: Boca Raton, **2012**; pp. 47–68.

[9] Crank, J. *The Mathemtics of Diffusion*, 2nd ed. Oxford University Press: Bristol, England, **1975**.

[10] Claussen, I. C.; Andresen, T.; Eikevik, T.; Strømmen, I. Atmospheric Freeze Drying -

Modeling and Simulation of a Tunnel Dryer. *Drying Technol.* **2007**, *25* (12), 1959–1965. DOI: 10.1080/07373930701727275.

[11] Wolff, E.; Gibert, H. Atmospheric Freeze-Drying Part 2: Modelling Drying Kinetics Using Adsorption Isotherms. *Drying Technol.* **1990**, *8* (2), 405–428. DOI: 10.1080/07373939008959891.

[12] Aseev, D. L.; Alexandrov, D. V. Directional solidification of binary melts with a non-equilibrium mushy layer. *Int. J. Heat Mass Tran.* **2006**, (49) 4903-4909 DOI: 10.1016/j.ijheatmasstransfer.2006.05.046.

[13] Worster, M. G. Convection in mushy layers. *Annu. Rev. Fluid Mech.* **1997**, (29) 91-122 DOI: 0066-4189/97/0115-0091.

[14] Warning, A. D.; Arquiza, J. M. R.; Datta, A. K. A Multiphase Porous Medium Transport Model with Distributed Sublimation Front to Simulate Vacuum Freeze Drying. *Food Bioprod. Process.* **2015**, *94* (August), 637–648. DOI: 10.1016/j.fbp.2014.08.011.

[15] Qin, R. S.; Bhadeshia, H. K. Phase field method. *J. Mater. Sci. Technol.* **2010**, 26 (7), 803-811. DOI: 10.1179/174328409X453190.

[16] Karma, A.; Rappel, W. Phase-field method for computationally efficient modeling of solidification with arbitrary interface kinetics. *Bull. Am. Phys. Soc.* **1996**, 53 (4) 3017-3020. DOI: 1063-651X/96/53(4)/3017(4).

[17] Ozuna, C.; Santacatalina, J. V; Mulet, A.; García-Pérez, J. V. Textural Properties of Vegetables: A Key Parameter on Ultrasonic Assisted Convective Drying. *Ultrason. Sonochem.* **2014**, *21* (May), 1235–1243.

[18] Velardi, S. A. Barresi, A. A. Development of simplified models for the freeze-drying process and investigation of the optimal operating conditions. *Chem. Eng. Res. Des.* **2008**, 86, 9-22. DOI: doi:10.1016/j.cherd.2007.10.007.

[19] Liapis, A. I.; Bruttini, R. Freeze Drying of Pharmaceutical Crystalline and Amorphous Solutes in Vials: Dynamic Multidimensional Models of the Primary and Secondary Drying Stages and Qualitative Features of the Moving Interface. *Drying Technol*. **1995**, *13* (1-2), 43-72. DOI: 10.1080/07373939508916942.

[20] Halder, A.; Dhall, A.; Datta, A. K. An Improved, Easily Implementable, Porous Media Based Model for Deep-Fat Frying Part I: Model Development and Input Parameters. *Food Bioprod. Process.* **2007**, *85* (C3), 209–219.

[21] Fang, G.; Ward, C. A. Temperature Measured Close to the Interface of an Evaporating Liquid. *Phys. Rev. E - Stat. Physics, Plasmas, Fluids, Relat. Interdiscip. Top.* **1999**, *59* (1), 417–428. DOI: 10.1103/physreve.59.417.

[22] Halder, A.; Dhall, A.; Datta, A. k. Modeling Transport in Porous Media With Phase Change: Applications to Food Processing. *J. Heat Transfer* **2010**, *133* (3), 1–13. DOI: 10.1115/1.4002463.

[23] Hahn, D.; Özisik, M. *Heat Conduction*, 3rd ed.; John Wiley & Sons: New York, **2012.**

[24] Russo, P.; Adiletta, G.; Di Matteo, M. The Influence of Drying Air Temperature on the Physical Properties of Dried and Rehydrated Eggplant. *Food Bioprod. Process.* **2013**, *91* (3), 249–256. DOI: 10.1016/j.fbp.2012.10.005.

[25] Fissore, D.; Pisano, R.; Barresi, A. A. Using Mathematical Modeling and Prior Knowledge for QbD in Freeze-Drying Processes, In *Quality by Design for Biopharmaceutical Drug Product Development*, F. Jameel et al., Eds. Springer Science: New York, **2015**; pp.565-593.

[26] Zhang, S.; Liu, J. Distribution of Vapor Pressure in the Vacuum Freeze-Drying Equipment. *Math. Probl. Eng.* **2012**, *2012*, 1–10. DOI: 10.1155/2012/921254.

[27] Fissore, D.; Pisano, R.; Barresi, A. A. On the Methods Based on the Pressure Rise Test for Monitoring a Freeze-Drying Process. *Drying Technol.* **2011**, *29* (1), 73–90.

DOI:10.1080/07373937.2010.482715.

[28] Fukusano, S. Thermophysical Properties of Ice, Snow, and Sea Ice. *Int. J. Thermophys.* **1990**, *11* (2), 353–371. DOI: 10.1007/bf01133567.

[29] Sereno, A. M.; Silva, M. A.; Mayor, L. Determination of Particle Density and Porosity in Foods and Porous Materials with High Moisture Content. *Int. J. Food Prop.* **2007**, *10* (3), 455–469. DOI: 10.1080/10942910600880736.

[30] Ali, S. D.; Ramaswamy, H. S.; Awuah, G. B. Thermo-Physical Properties of Selected Vegetables as Influenced by Temperature and Moisture Content. *J. Food Process Eng.* **2002**, *25* (5), 417–433. DOI: 10.1111/j.1745-4530.2002.tb00575.x.

[31] Nam, J. H.; Song, C. S. Numerical Simulation of Conjugate Heat and Mass Transfer during Multi-Dimensional Freeze Drying of Slab-Shaped Food Products. *Int. J. Heat Mass Transf.* **2007**, *50* (23–24), 4891–4900. DOI: 10.1016/j.ijheatmasstransfer.2007.08.004.

[32] Tchigeov, G. Thermophysical Processes in Food Refrigeration Technology. In *Food Industry*, Moskow, **1979**.

[33] USDA. *Nutrient Database for Standard Reference, Release 11*, Washington, D.C. , **1996.**

[34] Pikal, M. J.; Roy, M. L.; Shah, S. Mass and Heat Transfer in Vial Freeze-drying of Pharmaceuticals: Role of the Vial. *J. Pharm. Sci.* **1984**, *73* (9), 1224–1237. DOI: 10.1002/jps.2600730910.

[35] Rohsenow, W. M.; Hartnett, J. R. *Hand Book of Heat Transfer*, 3rd ed. McGraw-Hill: New York, **1998**.

[36] Howell, J. R.; Siegel, R.; Mengüç, M. P. *Thermal Radiation Heat Transfer,* 5th ed.; CRC Press, Taylor & Francis Group: Boca Raton, FL, **2010.**

[37] Incropera, F. P.; DeWitt, D. P.; Bergman, T. L.; Lavine, A. S. Radiation: Process and

Properties. In *Fundamentals of heat and mass transfer*, Hayton J., Ed. John Wiley & Sons: Hoboken, NJ, **2006**; pp. 724–809.

[38] Mittal, R.; Iaccarino, G. Immersed Boundary Methods. *Annu. Rev. Fluid Mech.* **2005**, *37* (1), 239–261. DOI: 10.1146/annurev.fluid.37.061903.175743.

[39] Hanson, P. M.; Yang, R. Y.; Tsou, S. C. S.; Ledesma, D.; Engle, L.; Lee, T. C. Diversity in Eggplant (Solanum Melongena) for Superoxide Scavenging Activity, Total Phenolics, and Ascorbic Acid. *J. Food Compos. Anal.* **2006**, *19*, 594–600. DOI: 10.1016/j.jfca.2006.03.001.

[40] Lietta, E.; Colucci, D.; Distefano, G.; Fissore, D. On the Use of Infrared Thermography for Monitoring a Vial Freeze-Drying Process. *J. Pharm. Sci.* **2018**, *108* (1), 391–398. DOI: 10.1016/j.xphs.2018.07.025.

[41] Patel, S. M.; Doen, T.; Pikal, M. J. Determination of End Point of Primary Drying in Freeze-Drying Process Control. *AAPS PharmSciTech* **2010**, *11* (1), 73–84. DOI: 10.1208/s12249-009-9362-7.

[42] Pisano, R.; Fissore, D.; Barresi, A. A. Heat Transfer in Freeze-Drying Apparatus. In *Developments in Heat Transfer*, Dos Santos Bernardes, M. A., Ed. InTech: Rijeka, Croatia, **2011**.

[43] Fissore, D.; Pisano, R. Computer-Aided Framework for the Design of Freeze-Drying Cycles: Optimization of the Operating Conditions of the Primary Drying Stage. *Processes* **2015**, *3* (2), 406–421. DOI:10.3390/pr3020406.

List of Tables

List of Figures

for the run #A2.

Figure 7. (A) Comparison between the experimentally measured temperature profiles at the surface of the product (■) and those obtained through process simulation in the run #B (-15°C and 20 Pa). The error bars represent the ±1°C error in the temperature measurement typical of the sensors used. (B) Comparison between the amount of residual ice in the product (left axis, dashed line), calculated with the mathematical model of the process, and the pressure ratio (right axis, solid line) for the run #B.

Figure 8. (A) Comparison between the experimentally measured temperature profiles at the surface of the product (solid line) and those obtained through process simulation (using the parameters estimated in run #A1, dashed line, or optimizing model parameters, symbols) in the run #C (0°C and 30 Pa). The error bars represent the ±1°C error in the temperature measurement typical of the sensors used. (B) Comparison between the amount of residual ice in the product (left axis) calculated with the mathematical model of the process (using the parameters estimated in run #A1, dashed line, or optimizing model parameters, symbols), and the pressure ratio (right axis, solid line) for the run #C.

Figure 9. Evolution of the ice fraction in the 2nd, 4th and 6th layer of the computational grid during run #A2 calculated using the average values of K_v and D_{eff} shown in Table 2.

Figure 10. Time evolution of the ice fraction in an axial section of the computational domain in three different instants of time along the primary drying.

Table 1

Ice properties			
λ	$2.839 \cdot 10^6$	J/kg	Ref. [36]
Vapor properties			

$c_{p,g}$	1505	J kg^{-1} K^{-1}	Ref. [14]
Dried product properties			
ϕ	0.74	-	
k_d	0.50	W m^{-1} K^{-1}	Experimentally measured values
$c_{p,d}$	2200	J kg^{-1} K^{-1}	
ρ_s	213	kg/m^{-3}	
Chamber characteristics			
Shelf width	0.45	m	
Shelf depth	0.45	m	
Space between shelves	0.20	m	

Table 2

	K_v, W m^{-2} $°C^{-1}$	D_{eff} x 10^4, m^2 s^{-1}
1st Profile	30.0	2.8
2nd Profile	28.0	2.7
3rd Profile	26.0	2.7
4th Profile	30.0	2.5
5th Profile	28.0	2.6
Mean value	28.4	2.66
Standard deviation	±6%	±4%

Figure 1

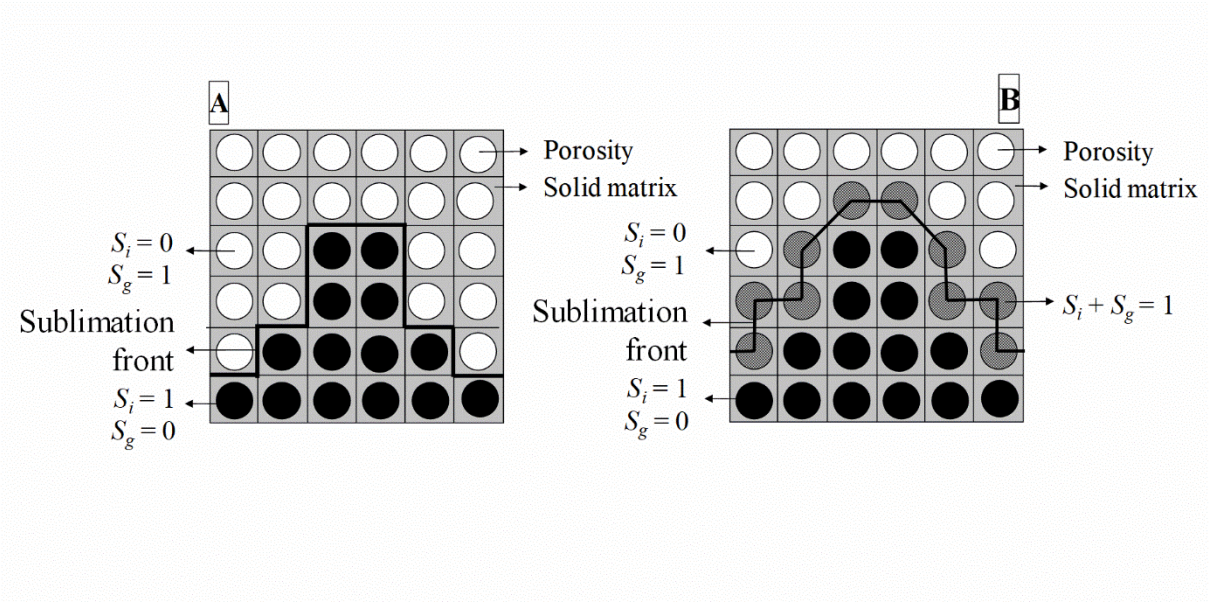
A
B
Porosity
Solid matrix
$S_i = 0$
$S_g = 1$
Sublimation
front
$S_i = 1$
$S_g = 0$
$S_i + S_g = 1$

Figure 2

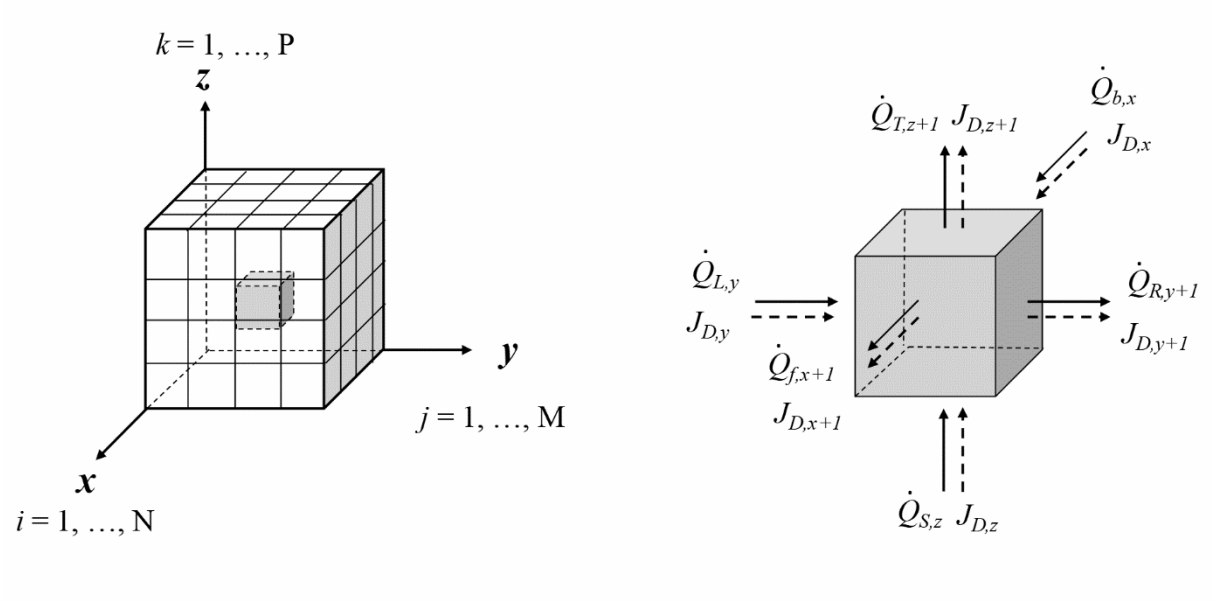
k = 1, …, P
z
y
j = 1, …, M
x
i = 1, …, N
$\dot{Q}_{T,z+1}$ $J_{D,z+1}$
$\dot{Q}_{b,x}$
$J_{D,x}$
$\dot{Q}_{L,y}$
$J_{D,y}$
$\dot{Q}_{R,y+1}$
$J_{D,y+1}$
$\dot{Q}_{f,x+1}$
$J_{D,x+1}$
$\dot{Q}_{S,z}$ $J_{D,z}$

Figure 3

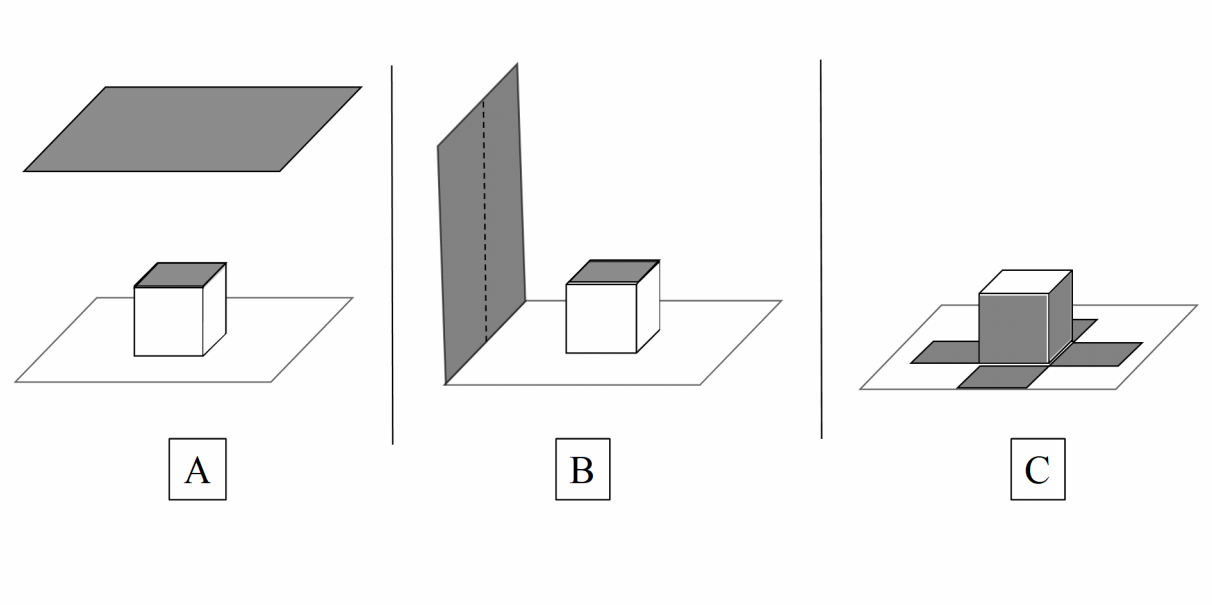

Figure 4

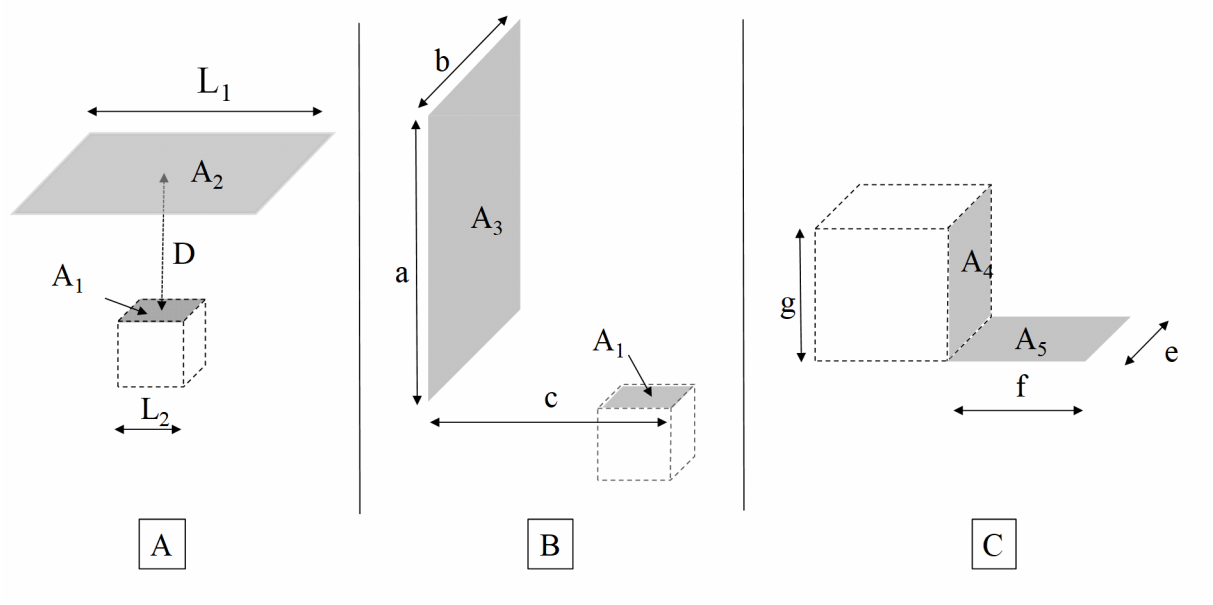

Figure 5

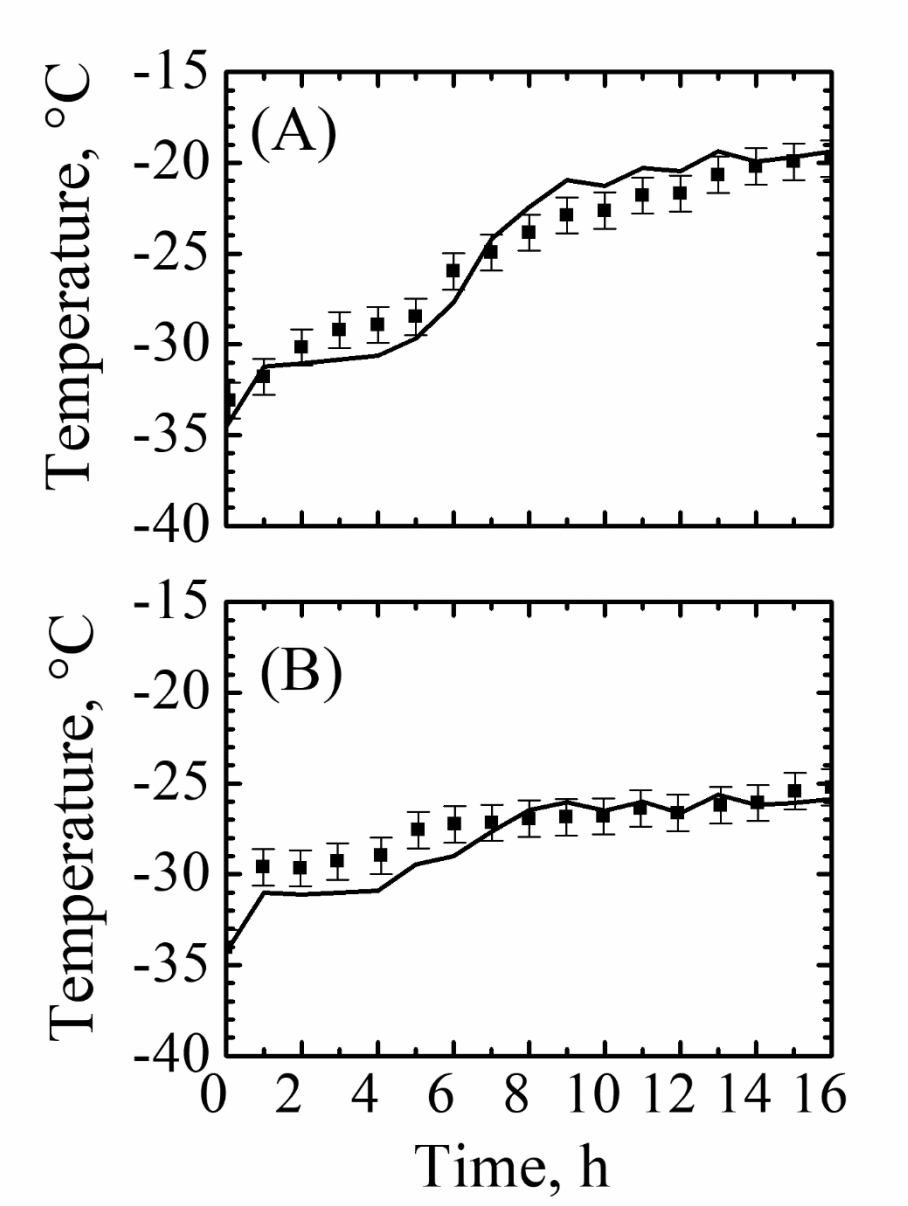
(A)
(B)
Temperature, °C
Temperature, °C
-15
-20
-25
-30
-35
-40
0
2
4
6
8
10
12
14
16
Time, h

Figure 6

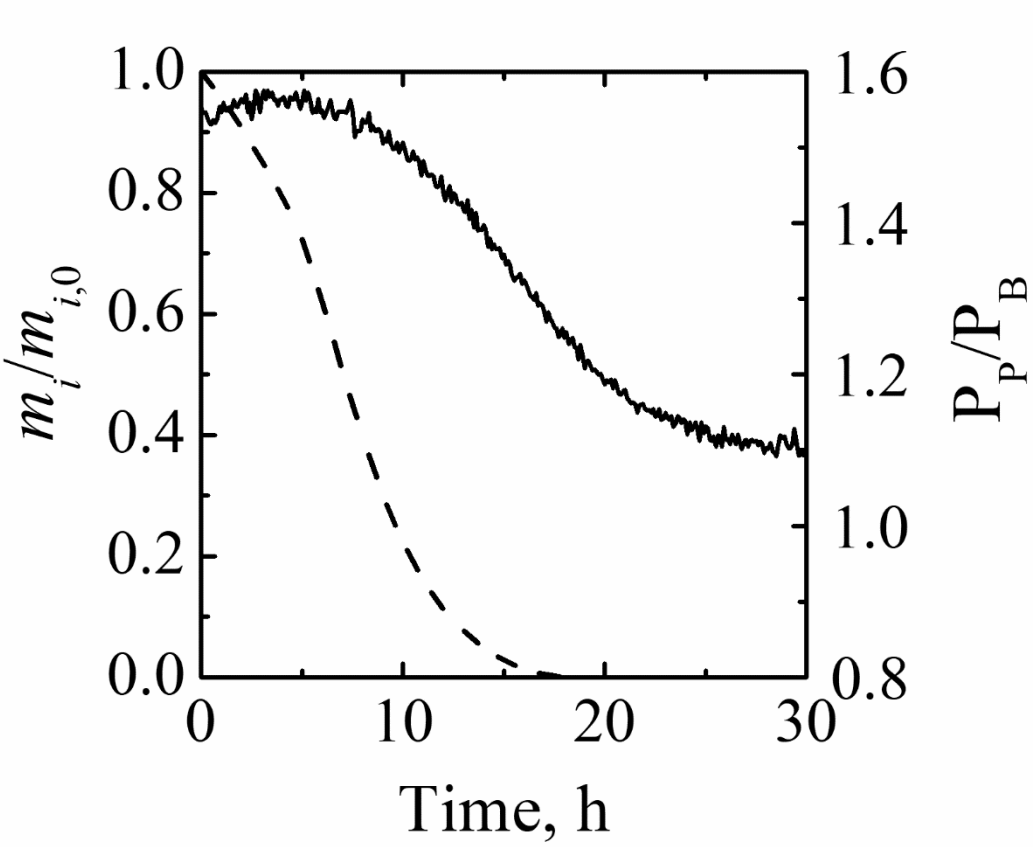

Figure 7

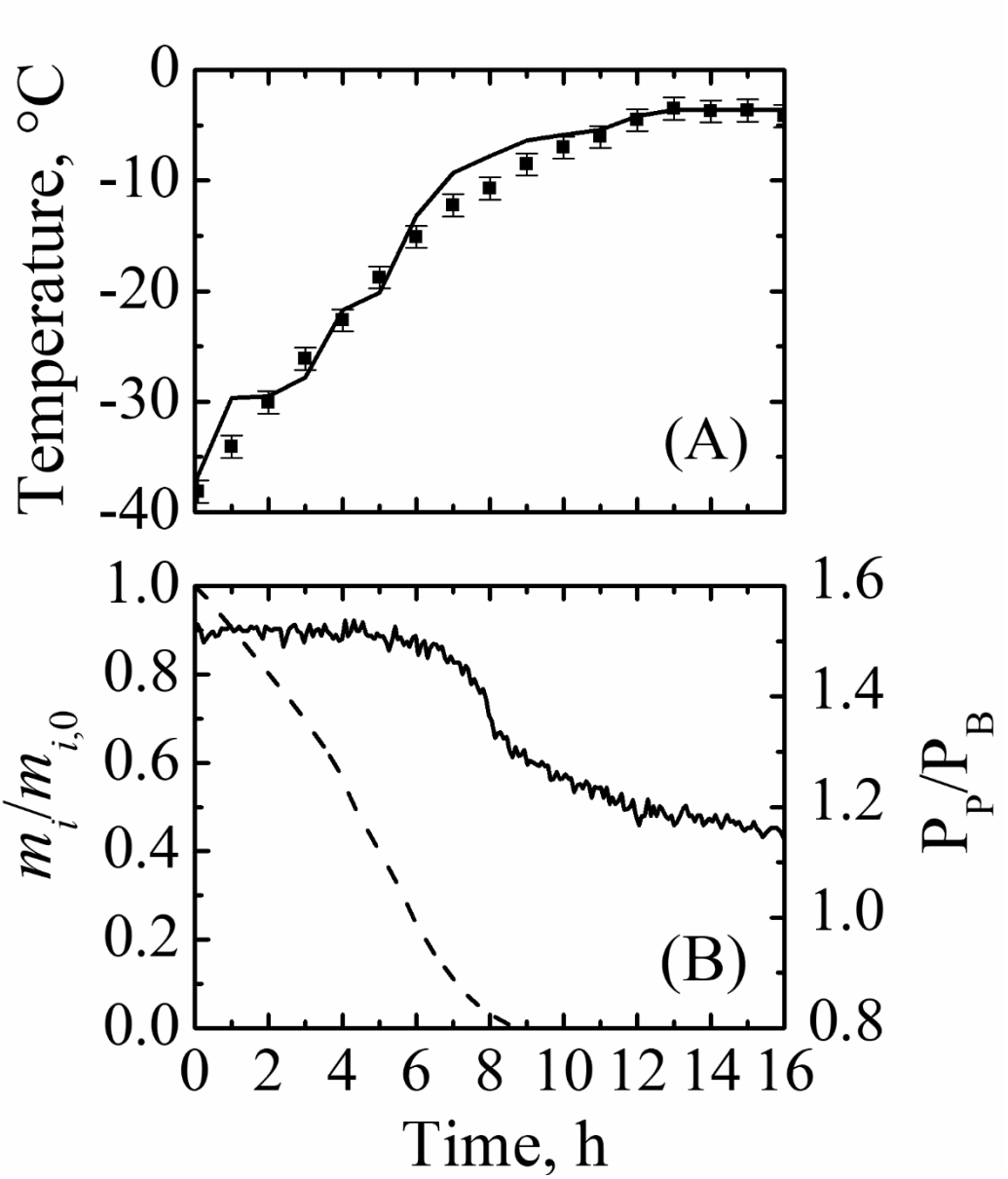
Temperature, °C
0
-10
-20
-30
-40
(A)
$m_i/m_{i,0}$
1.0
0.8
0.6
0.4
0.2
0.0
P_P/P_B
1.6
1.4
1.2
1.0
0.8
(B)
0 2 4 6 8 10 12 14 16
Time, h

Figure 8

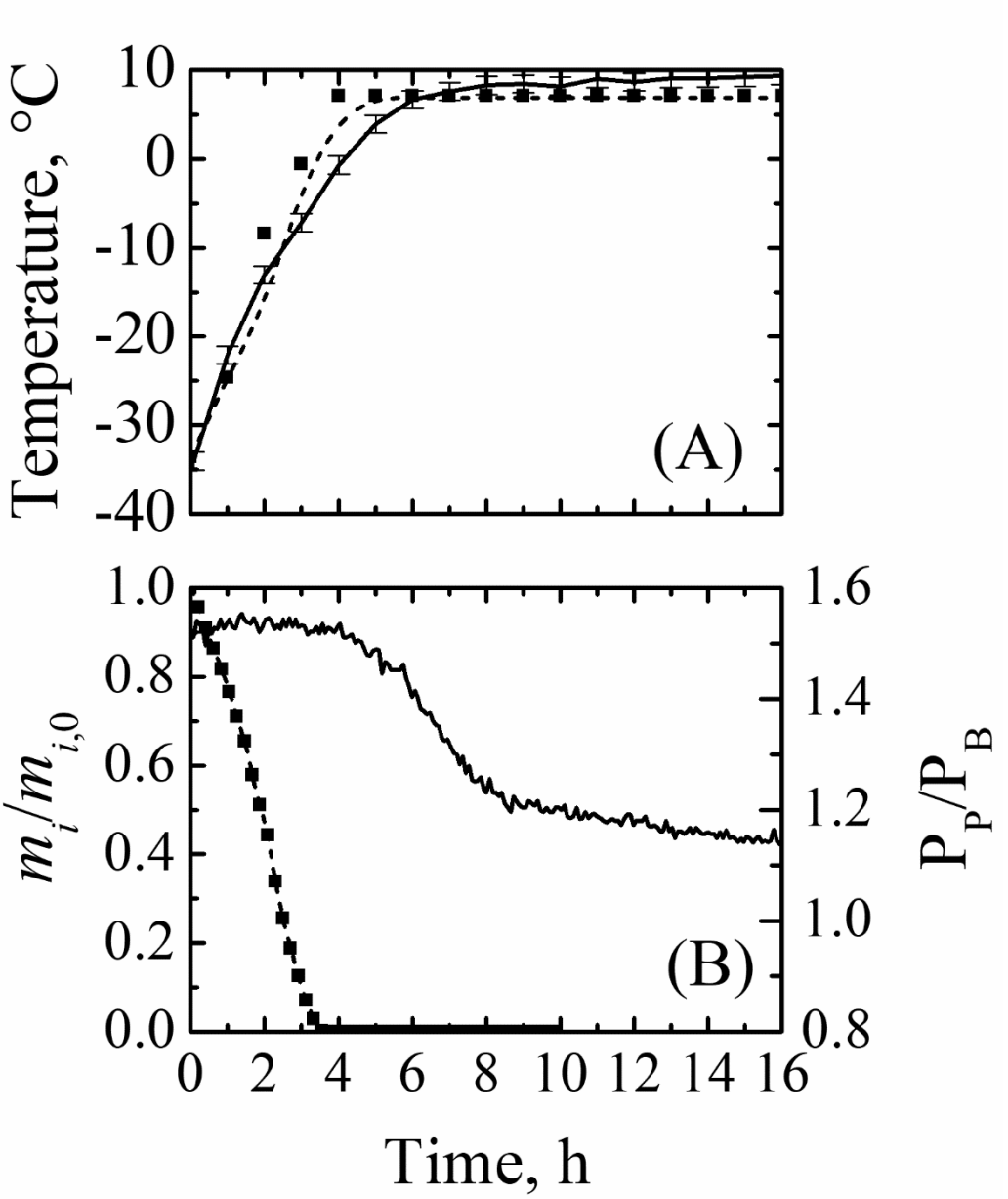
Temperature, °C
10
0
-10
-20
-30
-40
(A)
$m_i/m_{i,0}$
1.0
0.8
0.6
0.4
0.2
0.0
(B)
P_P/P_B
1.6
1.4
1.2
1.0
0.8
0 2 4 6 8 10 12 14 16
Time, h

Figure 9

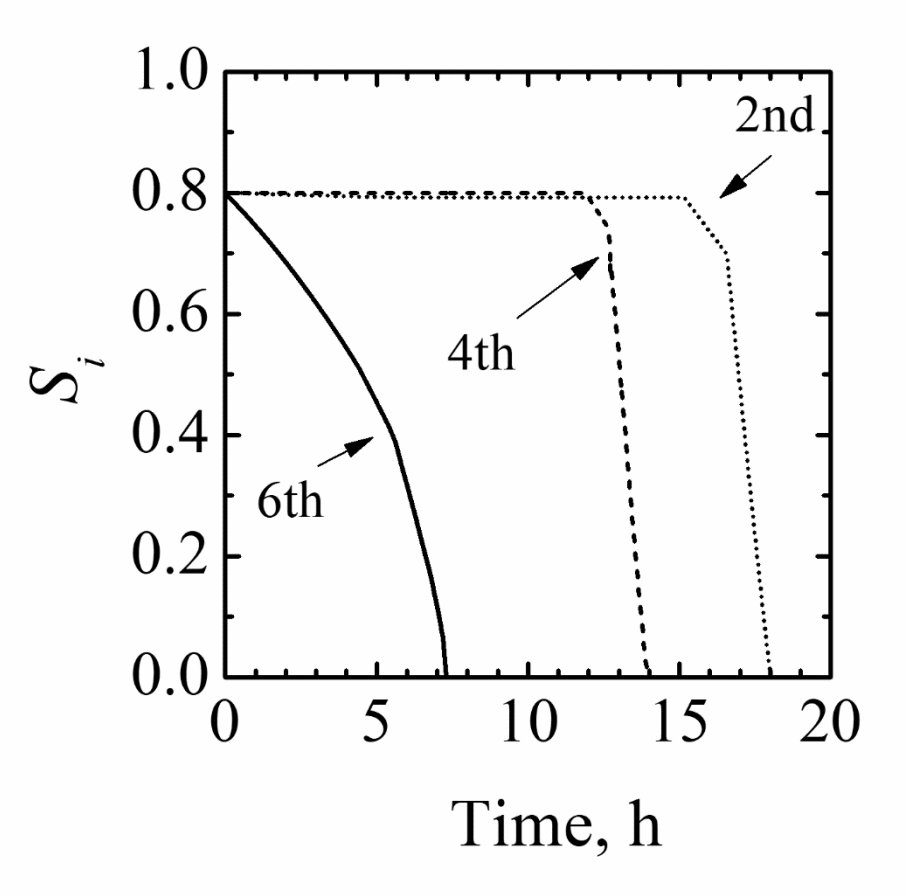

Figure 10